Estimating Transient Climate Response in a large-ensemble global climate model simulation

B.K. Adams and A.E. Dessler*
Dept. of Atmospheric Sciences, Texas A&M University, College Station, TX
* corresponding author, adessler@tamu.edu

Main points:

1. In a large model ensemble, we find that estimates of TCR from the 20th century tends to be low biased compared to the model's true TCR.
2. Internal variability can push down or enhance the warming in ensemble members & lead to large errors in TCR inferred from the 20th century.
3. We also verify that the details of the construction of the temperature dataset from which TCR is inferred can lead to significant biases in TCR inferred from observed warming.

Plain language summary:

The transient climate response (TCR) is defined to be the warming after 70 years of a 1% per year increase in atmospheric CO_2. It is one of the important metrics in climate science because it plays a key role in determining how much warming we will experience in the future. Previous work has found that TCR inferred from observed warming over the 20th century tends to be lower than TCR in climate models. This has been used by suggest that climate models are overpredicting future warming. We use a large number of climate model runs to investigate the methodology of this comparison. We find that TCR estimated from the 20th century simulations may indeed be much lower than the model's true TCR. This arises from biases in the methodology of estimating TCR from 20th century warming, as well as biases in the construction of the observational temperature data sets. We therefore find no evidence that models are overestimating TCR.

Abstract

The transient climate response (TCR), defined to be the warming in near-surface air temperature after 70 years of a 1% per year increase in CO_2, can be estimated from observed warming over the 19th and 20th centuries. Such analyses yield lower values than TCR estimated from global climate models (GCMs). This disagreement has been used to suggest that GCMs' climate may be too sensitive to increases in CO_2. Here we critically evaluate the methodology of the comparison using a large ensemble of a fully coupled GCM simulating the historical period, 1850–2005. We find that TCR estimated from model simulations of the historical period can be much lower than the model's true TCR, replicating the disagreement seen between observations and GCM estimates of TCR. This suggests that the disagreement could be explained entirely by the methodology of the comparison and undercuts the suggestions that GCMs overestimate TCR.

Introduction

The transient climate response (TCR) is frequently used to quantify the sensitivity of our climate system to increases in greenhouse gases. It is defined to be the warming in near-surface air temperature after 70 years of a 1% per year increase in atmospheric CO_2. As described below, it can be estimated from observed warming over the 19th and 20th centuries, yielding most-likely TCR values of 1.3-1.6 K [Bengtsson and Schwartz, 2013; Otto et al., 2013; Richardson et al., 2016; Lewis and Curry, 2018]. These values lie below the CMIP5 ensemble average TCR of 1.8 K [Forster *et al.*, 2013]. Resolving this disagreement may have important consequences for our confidence in the fidelity of climate models and their simulations of future climate change.

We will test the methodology of this comparison using a large model ensemble, an increasingly popular tool to study the impact of internal variability on the climate system. The most appropriate ensemble for this type of problem contains many runs of a single model with identical physics and external forcing but different initial conditions, which allows one to infer the impact of internal variability in the absence of inter-model differences. As each ensemble member evolves in time, internal variability of the different members is out of phase, leading to differences in the climate states among the ensemble members. In fact, one can think of our observational record as one member of a theoretical ensemble of Earth's climate trajectories. A model ensemble therefore gives us insight into what alternative climate histories may have looked like.

Data

We analyze output from an ensemble of 100 runs of the fully-coupled Max Planck Institute Earth System Model version 1.1 (MPI-ESM1.1) covering the period 1850-2005. The ensemble was used by Dessler et al. [2018] to characterize the impact of internal variability on estimates of the equilibrium climate sensitivity (ECS); they found that internal variability can lead to significant errors in ECS inferred from historical observations. Hedemann et al. [2017] analyzed this ensemble to determine potential causes of the so-called warming hiatus that occurred in the 2000s.

As described by Dessler et al. [2018]: "This is the latest coupled climate model from the Max Planck Institute for Meteorology and consists of the ECHAM6.3 atmosphere and land model coupled to the MPI-OM ocean model. The atmospheric resolution is T63 spectral truncation, corresponding to about 200 km, with 47 vertical levels, whereas the ocean has a nominal resolution of about 1.5 degrees and 40 vertical levels. MPI-ESM1.1 is a bug-fixed and improved version of the MPI-ESM used during CMIP5 [Giorgetta *et al.*, 2013] and nearly identical to the MPI-ESM1.2 … model being used to provide output to CMIP6, except that the historical forcings are from the MPI-ESM. Each of the 100 members simulates the years 1850-2005 (Fig. 1) and use the same evolution of historical natural and anthropogenic forcings. The members differ only in their initial conditions —each starts from a different state sampled from a 2000-year control simulation."

Dessler et al. further say: "We calculate effective radiative forcing F for the ensemble by subtracting top-of-atmosphere flux R in a run with climatological sea surface temperatures (SSTs) and a constant pre-industrial atmosphere from average R from an ensemble of three runs using the same SSTs but the time-varying atmospheric composition used in the historical runs [Hansen *et al.*, 2005; Forster *et al.*, 2016]. The three-member ensemble begins with perturbed atmospheric states."

We estimate F_{2xCO2} using the same approach in a set of fixed SST runs, one with a pre-industrial atmosphere and one in which CO_2 increases at 1% per year. F_{2xCO2} is then estimated as the average difference in top-of-atmosphere flux over years 62-78, which produces a value of 3.7 W/m^2. This is lower than the value used in Dessler et al. [2018], 3.9 W/m^2, which was estimated as one-half of the 4xCO_2 forcing from the same runs. Because of the slight non-linearity in the relation between forcing and the logarithm of CO_2, taking one half of the 4xCO_2 forcing is an overestimate of F_{2xCO2}.

We also analyze a 68-member ensemble of the MPI-ESM1.1 forced with CO_2 increasing at 1%/year (hereafter, “1% runs”). As with the historical ensemble, the 1% ensemble members differ only in their initial conditions — each starts from a different state sampled from a 2000-year pre-industrial control simulation.

Analysis of biases in TCR

Time series of global-average near-surface air temperature for all 100 members are plotted in Fig. 1 of Dessler et al. [2018]; that plot shows that the model ensemble is in good agreement with observed surface temperatures. TCR can be estimated from the ensemble’s temperature data with this equation [Gregory and Forster, 2008; Otto *et al.*, 2013; Richardson *et al.*, 2016]:

$$\mathrm{TCR}_{hist} = \Delta\mathrm{T}\,\frac{\mathrm{F}_{2\times\mathrm{CO2}}}{\Delta\mathrm{F}} \qquad (1)$$

where ΔT is the change in temperature over the historical period and ΔF is the change in radiative forcing. In our analysis, Δ represents the change between the 1859-1882 average, selected because it is not strongly influenced by volcanic eruptions [Mauritsen and Pincus, 2017; Lewis and Curry, 2018], and the average of the last ten years of the runs, 1996-2005. We refer to TCRs estimated this way as TCR_{hist}.

We first calculate TCR_{hist} in each ensemble member using global-average near-surface air temperature for ΔT. The calculated values range from 1.32 to 1.94 K (5-95% range 1.48-1.90 K) (Fig. 1a, Table 1). The spread in these TCR estimates is entirely due to internal variability and the spread is similar to previous estimates [Huber *et al.*, 2014; Hawkins *et al.*, 2016]. The standard deviation of ΔT from the ensemble is 0.07 K, close to that assumed by Lewis and Curry [2015], implying a similar spread in TCR due to internal variability in their analysis.

TCR is formally defined as the warming of global-average near-surface air temperature in response to CO_2 increasing at 1% per year, at the time of doubling. This value, which we will call TCR_{true}, can be estimated by averaging the warming (relative to pre-industrial) in years 60-80 of the 68-member ensemble of 1% runs. We find that TCR_{true} for the MPI-ESM1.1 is 1.78 K; this is 0.10 K (5.8%) larger than the average of the ensemble's TCR_{hist} (1.68 K).

Thus, TCR_{hist} is a low-biased estimate of TCR_{true} in the ensemble. The magnitude, and even the sign, of this bias varies depending on the portion of the historical record being examined (Table 1). Overall, though, we see a clear tendency for the TCR_{hist} to underestimate TCR_{true}. Previous papers have suggested that the biases in TCR_{hist} could be due to aerosol forcing efficacy [Kummer and Dessler, 2014; Shindell, 2014; Marvel *et al.*, 2015], although that explanation remains to be validated in this ensemble.

We are now in a position to critically evaluate previous comparisons of TCR from observations and GCMs. TCR estimated from observations, which are TCR_{hist}, have most-likely values in the range 1.3-1.6 K [Bengtsson and Schwartz, 2013; Otto *et al.*, 2013; Richardson *et al.*, 2016; Lewis and Curry, 2018], although the uncertainty in the individual estimates is large. The CMIP5 ensemble's TCR, which are TCR_{true}, fall in the range 1.8±0.6 K (average and 5-95% confidence interval) [Forster *et al.*, 2013]. Our analysis of the MPI-ESM1.1 ensemble demonstrates how a model with a TCR_{true} of 1.78 K might nevertheless produce TCR_{hist} in some ensemble members that that are much lower (1.3-1.4, Figure 1a) and in agreement with observational estimates.

We can also confirm previous suggestions that two issues with the observed ΔT, masking and blending, are further biasing TCR_{hist} to even lower values [Richardson *et al.*, 2016]. Masking refers to the fact that the observations are geographically incomplete, and that the degree of incompleteness has changed over time, leading to biases in global-average ΔT [Cowtan and Way, 2014]. To test the impact of this on TCR_{hist}, we also calculated ΔT in the ensemble using a time-varying mask derived from HadCRUT4 (v4.6.0.0) [Morice *et al.*, 2012]. Using this masked ΔT in Eq. 1, ensemble average TCR_{hist} drops from 1.68 K to 1.59 K (Fig. 1b, Table 2). However, this masking bias is bigger in some observational data sets than others. If we mask the ensemble's temperatures following the Berkeley Earth gridded land-ocean data set [Rohde *et al.*, 2013] we find a much smaller bias (Table 2).

The second issue is blending, which refers to the fact that observed ΔT data sets are usually a blend of near-surface air temperature over land and sea ice but sea surface temperature (SST) over open ocean. Because near-surface air temperature is warming faster than SSTs, this blending lowers ΔT compared to an estimate derived entirely from near-surface air temperature [Cowtan *et al.*, 2015; Santer *et al.*, 2000]. We test this by calculating a blended ΔT in the ensemble, which we also mask following HadCRUT4. Using this blended and masked ΔT, ensemble average TCR_{hist} drops to 1.47 K (Fig. 1d, Table 2). Masking with Berkeley Earth again provides a less-biased estimate, with ensemble average TCR_{hist} of 1.55 K (Table 2).

In these blending calculations, we calculate anomalies of the individual data sets first, and then combine them. We have also blended absolute temperatures and then calculated anomalies; we find that the order of calculation changes our results by less than 1% [Cowtan *et al.*, 2015]. Finally, we have also calculated blended ΔT using the temperature of the model's top ocean layer (representing the top 12 m of the ocean) instead of SST. Using that estimate of ΔT yields TCR_{hist} estimates that are similar to those that blend SST (Fig. 2f, Table 2).

Analysis of internal variability in the ensemble

The wildcard in this analysis is internal variability. Given that we have only one realization of the historical record, there is no way for us to know whether the warming over the historical period is less or greater than the average of all possible trajectories of our climate system over the historical period. Any deviation of the observed record from the "ensemble average" of the Earth's historical climate trajectory would lead directly to errors in TCR_{hist} estimated from observations. Our analysis shows that this variability could, by itself, explain the difference in TCR between observations and CMIP5 models [Lewis and Curry, 2015; Lewis and Curry, 2018; Richardson *et al.*, 2016].

The global and ensemble average ΔT is 0.84 K over the historical period. The spatial distribution (Fig. 2a and 2b) shows largest warming in the Arctic and least in the Southern Ocean (55°S).

The tropics (30°N-30°S) are responsible for 44% of the ensemble-average warming, the northern hemisphere extratropics (30°N-90°N) is responsible for 39%, and the southern hemisphere extratropics (30°S-90°S) is responsible for the rest, 17%.

The Berkeley observational record (Fig. 2c) shows a warming of 0.77 K over the same period, identical to the ensemble average of the model when the model data are blended and masked following the Berkeley data. However, the spatial distribution of the warming is slightly different (Fig. 2d), with more warming in the ensemble average in the northern polar region and west Pacific, and less elsewhere.

The pattern of surface warming varies among the members of the ensemble, which is what drives differences in the TCR. We can visualize this by plotting the covariance between the ensemble's 100 TCR values and the ensemble's 100 ΔT values at each grid point (Fig. 3). Most regions show positive covariances, meaning higher TCRs are associated with more warming almost everywhere.

But the covariance is not uniform — the spread in TCR arises mainly from ΔT variability in the northern hemisphere: 54% of the global average covariance comes from the northern hemisphere extratropics, 34% from the tropics (30°N-30°S), and 12% from the southern hemisphere extratropics. Previous work has shown that, for equilibrium climate sensitivity, the southern hemisphere plays the dominant role in variability in the ensemble [Dessler *et al.*, 2018], suggesting that variability in TCR and equilibrium climate sensitivity arise from different mechanisms.

High values of covariance in the northern hemisphere extratropics are found in the Arctic, especially the Barents Sea, as well as Northern Europe and the North Atlantic. The main contribution in the southern hemisphere extratropics is in the Weddell Sea, just to the east of the Antarctic Peninsula. Previous researchers have identified these regions as playing key roles in internal variability [Brown *et al.*, 2016; Martin *et al.*, 2013]. We are presently performing a more detailed analysis of the causes of internal variability in the ensemble that will be published in a future paper.

Conclusions

We have investigated why observation-based estimates of TCR tend to be lower than those from GCMs using a perfect model experiment. We have quantified a number of biases that can explain most, perhaps even all, of the disagreement: 1) a bias between TCR_{hist} and TCR_{true}, 2) a bias due to incomplete spatial coverage in the observational ΔT record, and 3) a bias due to the observational ΔT values being blends of air temperature and SSTs. These three biases are all acting in the same direction, to push TCR_{hist} to lower values. The impact of internal variability, which can suppress warming in some members of the ensemble, thereby further reducing TCR_{hist}, has a potentially large magnitude and therefore could also be playing a major role in the model-observation difference.

The uncertainty in individual estimates of TCR_{hist} from observations are large and the uncertainty range easily covers most of the TCR_{true} values from the CMIP5 ensemble [Lewis and Curry, 2015; Lewis and Curry, 2018; Richardson *et al.*, 2016]. Because of the large uncertainty in other parameters (e.g., aerosol forcing), adding uncertainty due to the issues we discuss in this paper will produce only nominal increases in the total uncertainty of the observational estimates. However, the biases we have investigated are capable of explaining the entire disagreement between the central values of the estimates, which has been the focus of much of the discussion.

Our work also informs how future analyses should be done. First, analyses should account for the role of internal variability, most likely by comparing observations to an ensemble of runs. In addition, we should not compare TCR_{hist} derived from observations to TCR_{true} — unless one can quantify and adjust for the bias between these methods. A better approach would be to compare TCR_{hist} from observations to TCR_{hist} derived from an ensemble of runs of the GCMs covering the same period as the observations. Finally, one must account for biases in the observations of ΔT used to estimate the observational TCR_{hist} by using masked and blended ΔT fields from the model to estimate the model-derived TCR_{hist}.

Acknowledgments: This work was supported by NSF grant AGS-1661861 to Texas A&M University. We thank the Bjorn Stevens, Thorsten Mauritsen, and Chris Hedemann of the Max-

Planck-Institut für Meteorologie for their help interpreting output from the ensemble that formed the basis of this analysis. We also thank Mark Richardson for his suggestions on the manuscript. Data and code are available from https://zenodo.org/record/1646854.

References

Bengtsson, L., & S. E. Schwartz (2013), Determination of a lower bound on Earth's climate sensitivity, Tellus B: Chemical and Physical Meteorology, 65, 21533, doi: 10.3402/tellusb.v65i0.21533.

Brown, P. T., W. Li, J. H. Jiang, & H. Su (2016), Spread in the magnitude of climate model interdecadal global temperature variability traced to disagreements over high-latitude oceans, Geophys. Res. Lett., 43, 12,543-512,549, doi: 10.1002/2016GL071442.

Cowtan, K., & R. G. Way (2014), Coverage bias in the HadCRUT4 temperature series and its impact on recent temperature trends, Q. J. R. Meteor. Soc., 140, 1935-1944, doi: doi:10.1002/qj.2297.

Cowtan, K., Z. Hausfather, E. Hawkins, P. Jacobs, M. E. Mann, S. K. Miller, et al. (2015), Robust comparison of climate models with observations using blended land air and ocean sea surface temperatures, Geophys. Res. Lett., 42, 6526-6534, doi: 10.1002/2015GL064888.

Dessler, A. E., T. Mauritsen, & B. Stevens (2018), The influence of internal variability on Earth's energy balance framework and implications for estimating climate sensitivity, Atmos. Chem. Phys., 18, 5147-5155, doi: 10.5194/acp-18-5147-2018.

Forster, P. M., T. Andrews, P. Good, J. M. Gregory, L. S. Jackson, & M. Zelinka (2013), Evaluating adjusted forcing and model spread for historical and future scenarios in the CMIP5 generation of climate models, Journal of Geophysical Research: Atmospheres, 118, 1139-1150, doi: 10.1002/jgrd.50174.

Forster, P. M., T. Richardson, A. C. Maycock, C. J. Smith, B. H. Samset, G. Myhre, et al. (2016), Recommendations for diagnosing effective radiative forcing from climate models for CMIP6, J. Geophys. Res., 121, 12460-12475, doi: 10.1002/2016jd025320.

Giorgetta, M. A., J. Jungclaus, C. H. Reick, S. Legutke, J. Bader, M. Böttinger, et al. (2013), Climate and carbon cycle changes from 1850 to 2100 in MPI-ESM simulations for the Coupled Model Intercomparison Project phase 5, Journal of Advances in Modeling Earth Systems, 5, 572-597, doi: 10.1002/jame.20038.

Gregory, J. M., & P. M. Forster (2008), Transient climate response estimated from radiative forcing and observed temperature change, J. Geophys. Res., 113, doi: 10.1029/2008jd010405.

Hansen, J., M. Sato, R. Ruedy, L. Nazarenko, A. Lacis, G. A. Schmidt, et al. (2005), Efficacy of climate forcings, Journal of Geophysical Research: Atmospheres, 110, doi: 10.1029/2005JD005776.

Hawkins, E., R. S. Smith, J. M. Gregory, & D. A. Stainforth (2016), Irreducible uncertainty in near-term climate projections, Climate Dynamics, 46, 3807-3819, doi: 10.1007/s00382-015-2806-8.

Hedemann, C., T. Mauritsen, J. Jungclaus, & J. Marotzke (2017), The subtle origins of surface-warming hiatuses, Nature Clim. Change, 7, 336-339, doi: 10.1038/nclimate3274.

Huber, M., U. Beyerle, & R. Knutti (2014), Estimating climate sensitivity and future temperature in the presence of natural climate variability, Geophys. Res. Lett., 41, 2086-2092, doi: 10.1002/2013GL058532.

Kummer, J. R., & A. E. Dessler (2014), The impact of forcing efficacy on the equilibrium climate sensitivity, Geophys. Res. Lett., 41, 3565-3568, doi: 10.1002/2014gl060046.

Lewis, N., & J. A. Curry (2015), The implications for climate sensitivity of AR5 forcing and heat uptake estimates, Climate Dynamics, 45, 1009-1023, doi: 10.1007/s00382-014-2342-y.

Lewis, N., & J. Curry (2018), The impact of recent forcing and ocean heat uptake data on estimates of climate sensitivity, J. Climate, doi: 10.1175/jcli-d-17-0667.1.

Martin, T., W. Park, & M. Latif (2013), Multi-centennial variability controlled by Southern Ocean convection in the Kiel Climate Model, Climate Dynamics, 40, 2005-2022, doi: 10.1007/s00382-012-1586-7.

Marvel, K., G. A. Schmidt, R. L. Miller, & L. S. Nazarenko (2015), Implications for climate sensitivity from the response to individual forcings, Nature Climate Change, 6, 386, doi: 10.1038/nclimate2888.

Mauritsen, T., & R. Pincus (2017), Committed warming inferred from observations, Nature Climate Change, 7, 652-655, doi: 10.1038/nclimate3357.

Morice, C. P., J. J. Kennedy, N. A. Rayner, & P. D. Jones (2012), Quantifying uncertainties in global and regional temperature change using an ensemble of observational estimates: The HadCRUT4 data set, J. Geophys. Res., 117, doi: 10.1029/2011jd017187.

Otto, A., F. E. L. Otto, O. Boucher, J. Church, G. Hegerl, P. M. Forster, et al. (2013), Energy budget constraints on climate response, Nature Geoscience, 6, 415-416, doi: 10.1038/ngeo1836.

Richardson, M., K. Cowtan, E. Hawkins, & M. B. Stolpe (2016), Reconciled climate response estimates from climate models and the energy budget of Earth, Nature Clim. Change, 6, 931-935, doi: 10.1038/nclimate3066.

Rohde, R., R. A. Muller, R. Jacobsen, E. Muller, S. Perlmutter, A. Rosenfeld, et al. (2013), A new estimate of the average earth surface land temperature spanning 1753 to 2011, Geoinfor. Geostat.: An Overview, 1, doi: 10.4172/2327-4581.1000101.

Santer, B. D., T. M. L. Wigley, D. J. Gaffen, L. Bengtsson, C. Doutriaux, J. S. Boyle, et al. (2000), Interpreting differential temperature trends at the surface and in the lower troposphere, Science, 287, 1227.

Shindell, D. T. (2014), Inhomogeneous forcing and transient climate sensitivity, Nature Climate Change, 4, 274, doi: 10.1038/nclimate2136.

Table 1. TCR_{hist} calculated with different base and end periods

base period	end period	average (K)	Full TCR range (K)	5-95% TCR range (K)	width (K)	% diff from true TCR	ΔF (W/m^2)
1859-1882	1940-1949	1.82	0.63-2.88	1.15-2.50	1.35	2.0	0.54
1859-1882	1951-1960	1.96	1.10-3.13	1.32-2.67	1.34	9.2	0.59
1859-1882	1969-1978	1.71	1.01-2.91	1.24-2.24	0.99	-4.0	0.81
1859-1882	**1996-2005**	**1.68**	**1.32-1.94**	**1.48-1.90**	**0.42**	-5.9	**1.85**
1930-1939	1996-2005	1.65	0.97-2.07	1.35-1.99	0.64	-7.9	1.41
1940-1949	1996-2005	1.62	1.02-2.16	1.28-2.04	0.76	-9.6	1.31
1951-1960	1996-2005	1.55	0.91-2.04	1.20-1.90	0.70	-14.8	1.26
1970-1979	1996-2005	1.67	0.99-2.42	1.20-2.09	0.90	-6.6	0.99

The bold line is the case primarily discussed in the text. Width is the difference between the 5^{th} and 95^{th} percentile values; % difference is average TCR_{hist} minus TCR_{true}, 1.78 K, divided by average TCR_{hist},, in percent; ΔF is the change in forcing between the base and end periods.

Table 2. TCR_{hist} calculated with different versions of ΔT

T_S data set	Description	average (K)	% diff from True TCR	Full TCR range (K)	5-95% TCR range (K)
TCR	**ΔT is global-average near-surface air temperature**	1.68	-5.9	1.32-1.94	1.48-1.90
TCR_masked_h	Same as TCR, but geographic coverage follows HadCRUT4	1.59	-11.8	1.23-1.85	1.40-1.80
TCR_masked_b	Same as TCR, but geographic coverage follows Berkeley Earth	1.67	-6.5	1.30-1.93	1.48-1.89
TCR_blend	ΔT is a blend of near-surface air temperature over land and sea ice and SSTs over open ocean	1.56	-14.2	1.21-1.82	1.37-1.77
TCR_blend_masked_h	Same as TCR_blend, but geographic coverage follows HadCRUT4	1.47	-21.4	1.12-1.72	1.28-1.67
TCR_blend_masked_b	Same as TCR_blend, but geographic coverage follows Berkeley Earth	1.55	-14.7	1.19-1.80	1.36-1.77
TCR_blend_oc	ΔT is a blend of near-surface air temperature over land and sea ice; elsewhere, use temperature of the top 12 m of the ocean	1.53	-16.6	1.19-1.78	1.34-1.73
TCR_blend_oc_masked_h	Same as TCR_blend_oc, but geographic coverage follows HadCRUT4	1.44	-23.7	1.10-1.69	1.25-1.64
TCR_blend_oc_masked_b	Same as TCR_blend_oc, but geographic coverage follows Berkeley Earth	1.51	-17.7	1.17-1.76	1.33-1.73

The bold line is the base case primarily discussed in the text; % difference is average TCR_{hist} minus TCR_{true}, 1.78 K, divided by average TCR_{hist}, in percent.

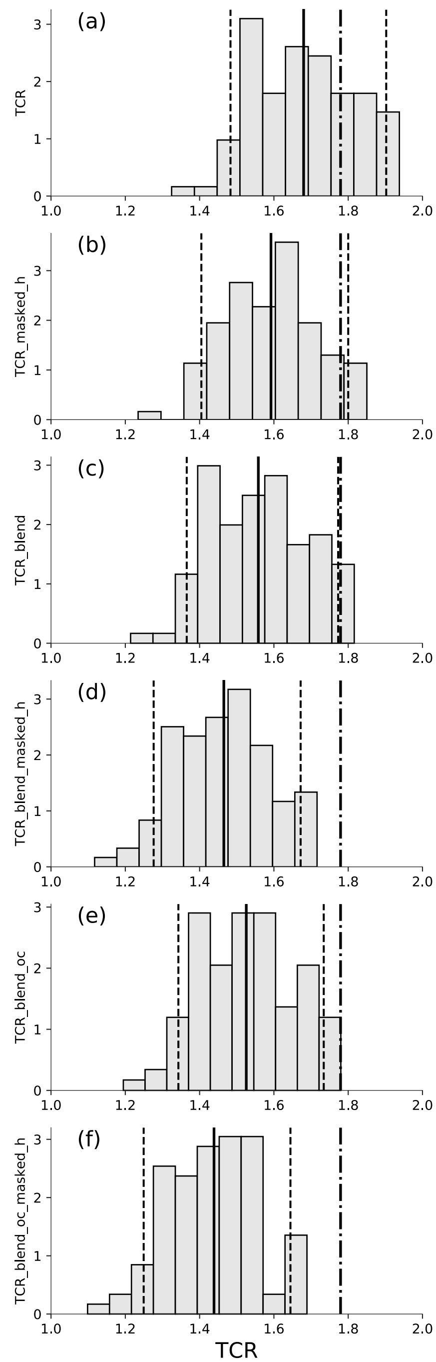

Figure 1. Histograms of TCR_{hist} (K) from the ensemble. Each panel shows the calculation with a different version of ΔT; see Table 2 for definitions. The solid black line represents the average, the dashed lines are the 5th and 95th percentiles. The dot-dashed line is TCR_{true} of the model, 1.78 K.

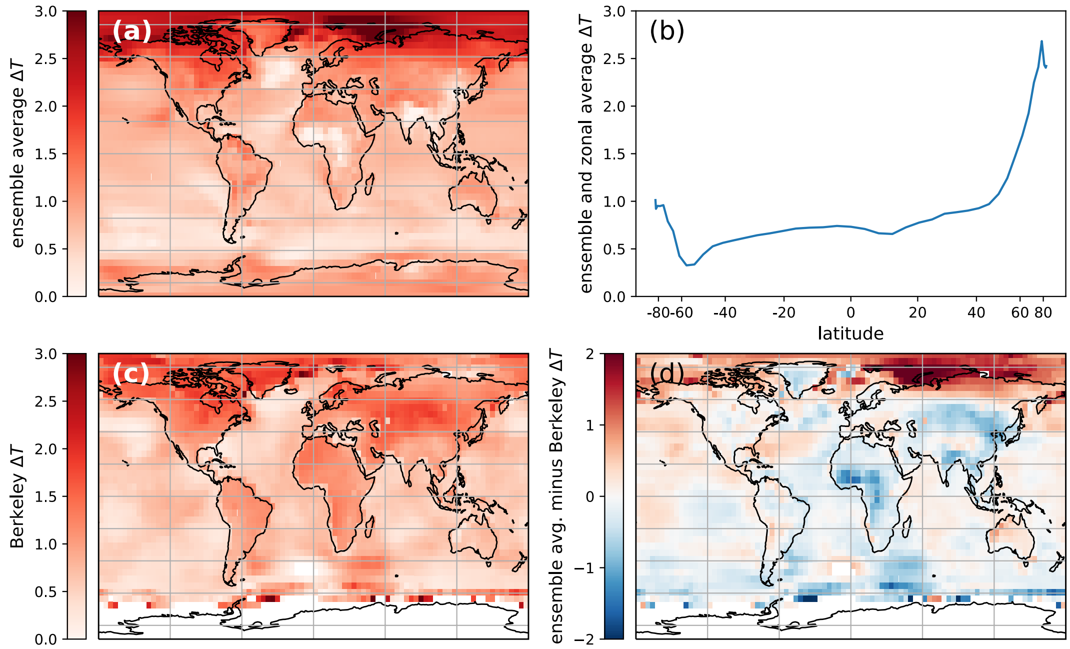

Figure 2. (a) Spatial distribution of ensemble average ΔT (near surface air temperature) (K), the average change in temperature between 1859-1882 and 1996-2005; (b) zonal average of the ensemble average ΔT vs. area-weighted latitude; (c) ΔT derived from Berkeley surface temperature data; (d) ΔT from the model, blended and masked following the Berkeley data set, minus ΔT derived from Berkeley data.

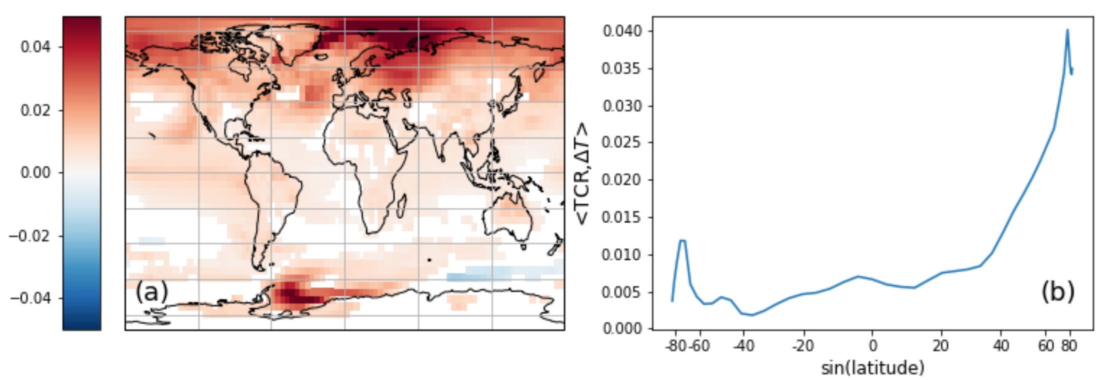

Figure 3. (a) Covariance of the ensemble's TCR and each grid point's ΔT (K^2); regions where the covariance is not statistically different from zero (5-95% confidence interval, estimated by a bootstrap technique) are white. (b) Covariance of TCR and zonal average ΔT (K^2).